

## **Axial gradient excitation accelerates volumetric imaging of two-photon microscopy**

**YUFENG GAO<sup>1,2,†</sup>, XIANYUAN XIA<sup>1,2,†</sup>, LINA LIU<sup>1,2</sup>, TING WU<sup>1,2</sup>, TINGAI CHEN<sup>1,2</sup>, JIA YU<sup>1,2</sup>, ZHILI XU<sup>3</sup>, LIANG WANG<sup>1,2</sup>, FEI YAN<sup>3</sup>, ZHUO DU<sup>4,5</sup>, JUN CHU<sup>1,2</sup>, YANG ZHAN<sup>6</sup>, BO PENG<sup>7</sup>, HUI LI<sup>1,2</sup>, WEI ZHENG<sup>1,2</sup>**

*<sup>1</sup>Research Center for Biomedical Optics and Molecular Imaging, Shenzhen Key Laboratory for Molecular Imaging, Guangdong Provincial Key Laboratory of Biomedical Optical Imaging Technology, Shenzhen Institute of Advanced Technology, Chinese Academy of Sciences, Shenzhen 518055, China*

*<sup>2</sup>CAS Key Laboratory of Health Informatics, Shenzhen Institute of Advanced Technology, Chinese Academy of Sciences, Shenzhen 518055, China*

*<sup>3</sup>Paul C. Lauterbur Research Center for Biomedical Imaging, Institute of Biomedical and Health Engineering, Shenzhen Institute of Advanced Technology, Chinese Academy of Sciences, Shenzhen, 518055, China*

*<sup>4</sup>State Key Laboratory of Molecular Developmental Biology, Institute of Genetics and Developmental Biology, Chinese Academy of Sciences, Beijing 100101, China*

*<sup>5</sup>Key Laboratory of Genetic Network Biology, Institute of Genetics and Developmental Biology, Chinese Academy of Sciences, Beijing 100101, China*

*<sup>6</sup>Brain Cognition and Brain Disease Institute, Shenzhen Institute of Advanced Technology, Chinese Academy of Sciences, Shenzhen 518055, China*

*<sup>7</sup>Centre for Micro Nano Systems and Bionic Medicine, Shenzhen Institute of Advanced Technology, Chinese Academy of Sciences, Shenzhen 518055, China*

*<sup>†</sup> These authors contributed equally to this work*

*[hui.li@siat.ac.cn](mailto:hui.li@siat.ac.cn)*

*[zhengwei@siat.ac.cn](mailto:zhengwei@siat.ac.cn)*

# Contents

- Fig. S1.** Theoretical and experimentally measured lateral resolutions.
- Fig. S2.** Axial localization error analysis on experimental data of Fig. 1c.
- Fig. S3.** Phototoxicity assessment.
- Fig. S4.** Simulated gradient foci with different lengths.
- Fig. S5.** Evaluation of axial overlap of different types of cellular structures.
- Fig. S6.** Gradient two-photon excitation microscope setup.
- Fig. S7.** Gradient focus generation flowchart
- Fig. S8.** Simulated gradient focus pair.
- Fig. S9.** Experimental gradient focus pair measured using 1- $\mu$ m-diameter fluorescent beads.
- Fig. S10.** Flowchart for axial location information extraction.
- Table S1.** Data acquisition parameters.

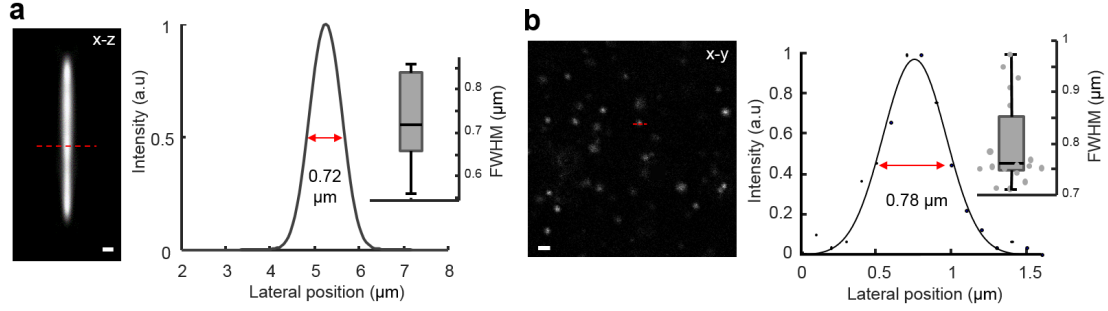


**Fig. S1** Theoretical and experimentally measured lateral resolutions. **(a)** Left, square of simulated point spread function of Grad-TPM (PSF<sup>2</sup>). Scale bar, 1 μm. Right, lateral profile across middle of PSF<sup>2</sup> (dashed red line on left panel), and statistical result of lateral resolutions calculated from different depths of PSF<sup>2</sup>. Squaring is necessary because intensity of two-photon excitation fluorescence is proportional to square of excitation intensity. **(b)** Left, exemplary image of 100-nm-diameter yellow-green fluorescence beads in gel used for measuring actual resolution of Grad-TPM system. Scale bar, 2 μm. Right, profile across middle of representative bead (dashed red line on left panel) with corresponding Gaussian fitting result and statistical result of lateral resolutions calculated from different beads ( $n = 20$ ).

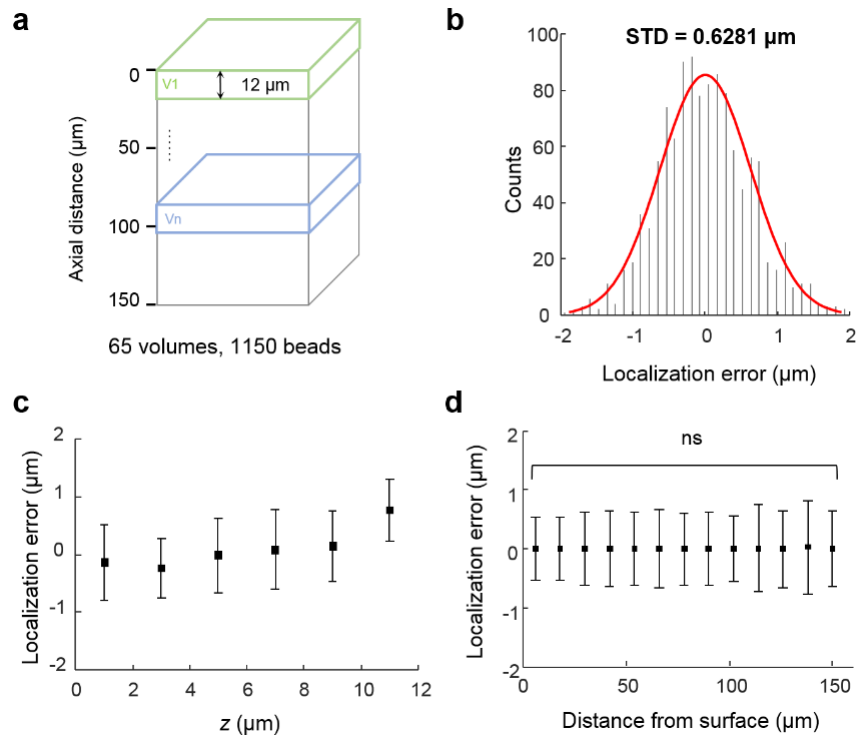


**Fig. S2** Axial localization error analysis on experimental data of Fig. 1c. **(a)** Imaging volume of the experimental data. **(b)** Histogram of the localization error. **(c)** Localization error as a function of depth in a single Grad-TPM volume. **(d)** Localization error as a function of the distance from sample surface.

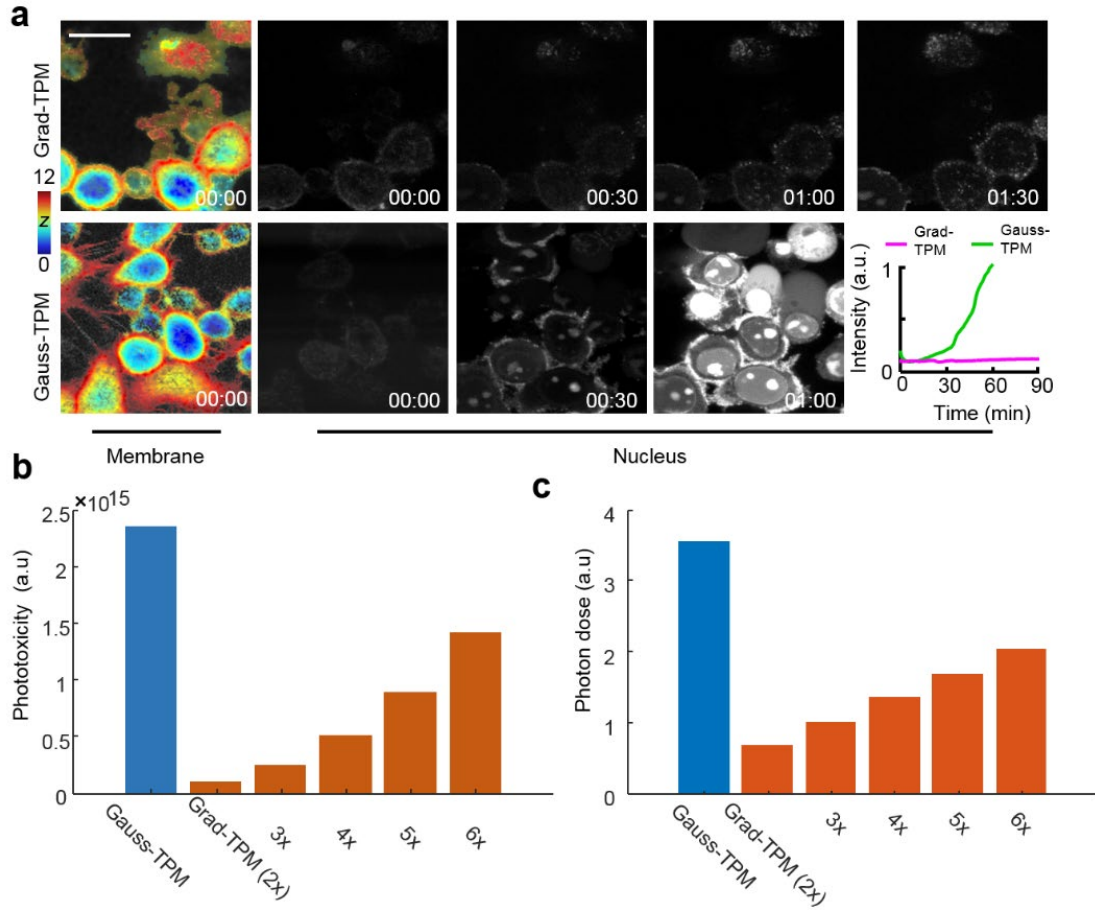


**Fig. S3** Phototoxicity assessment. **(a)** Time-lapse imaging on living HepG2 cells via Grad-TPM shows observably lower phototoxicity compared with traditional Gauss-TPM. Cell membrane and nucleus were labeled with DyLight 488 and PI, respectively. PI cannot cross the membrane of live cells and appear bright only if it binds to the nucleic acids after the cell is dead. Lower right graph is created by calculating average intensity of entire nucleus image at each time point. Scale bars, 20  $\mu\text{m}$ . Time is shown at corner as h:min. Units of  $z$ :  $\mu\text{m}$ . **(b)** Theoretical phototoxicity comparison of Grad-TPM and Gauss-TPM. 2-6 $\times$  indicate that excitation power of Grad-TPM is two to six times that of the Gauss-TPM. **(c)**, Theoretical photon-dose comparison. In TPM, phototoxicity and photon dose has been shown to scale as  $\int I(\vec{x}, t)^{2.5} dV dt$  and  $\int I(\vec{x}, t) dV dt$ , respectively, where  $I(\vec{x}, t)$  is the intensity distribution,  $V$  the excited volume, and  $t$  the time.

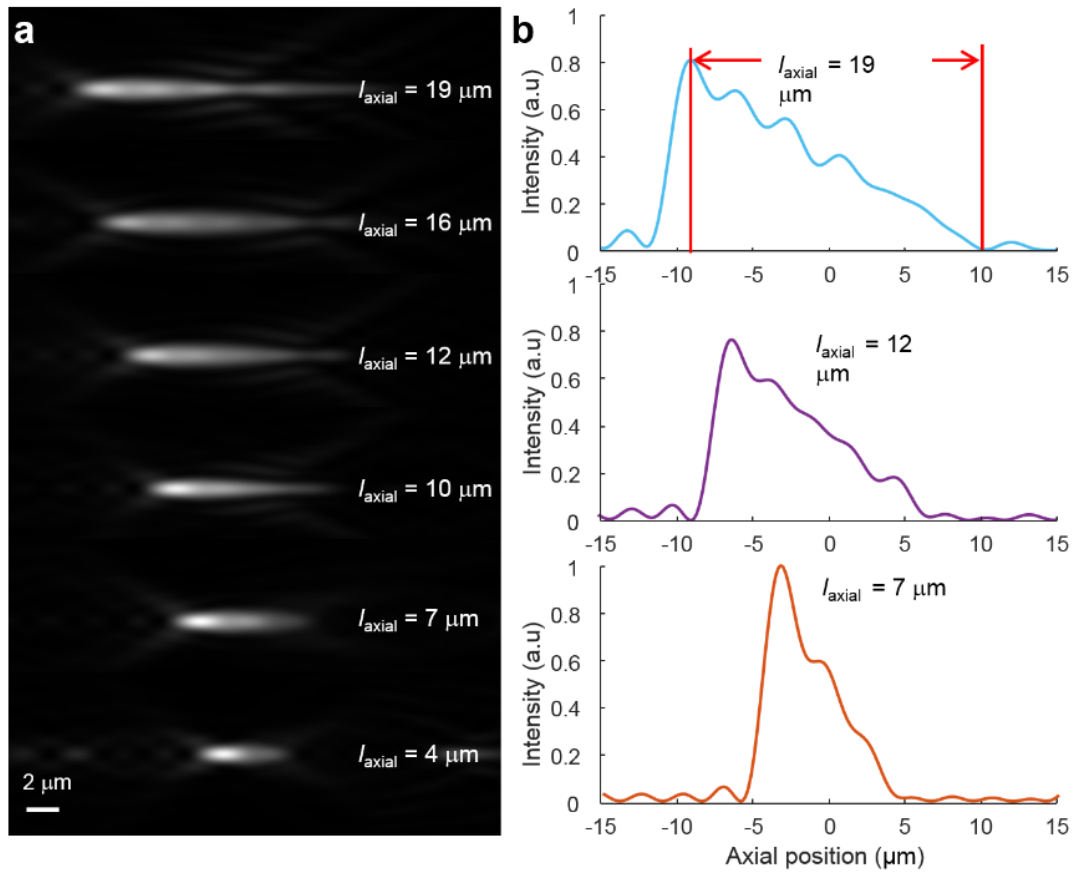


**Fig. S4** Gradient foci with different lengths. **(a)** Theoretical intensity distributions calculated using Richards–Wolf theory and varied from 4 to 20 in focal region. Scale bar, 2  $\mu\text{m}$ . **(b)** Corresponding profiles of 7, 12, and 19  $\mu\text{m}$  gradient foci along optical axis. These profile indicate that 12  $\mu\text{m}$  is favorable for Grad-TPM considering smoothness of slope, maximum intensity, and focal length.

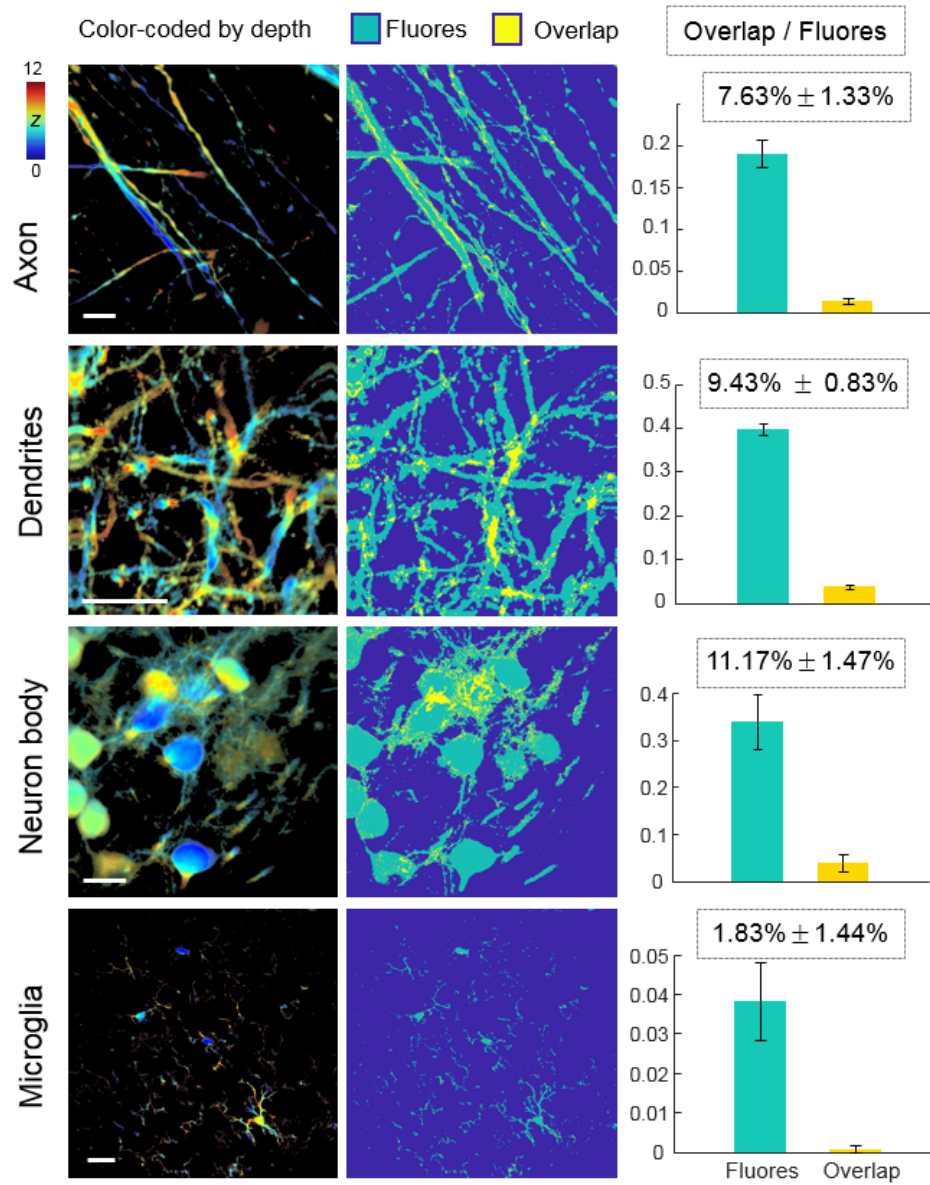


**Fig. S5** Evaluation of the axial overlap of different cellular structures in brain slices. Fluores: fluorescent structures; Overlap, where two or more structures overlaps within the 12- $\mu$ m axial range. The ratio of the overlap area to the total fluorescent area (measured on Guass-TPM images) ranges from 1.83% to 11.17%, suggesting that many structures are sparsely distributed in the 12- $\mu$ m axial range. Therefore, the Grad-TPM method is suitable for imaging brains slices. Unit of z:  $\mu$ m.

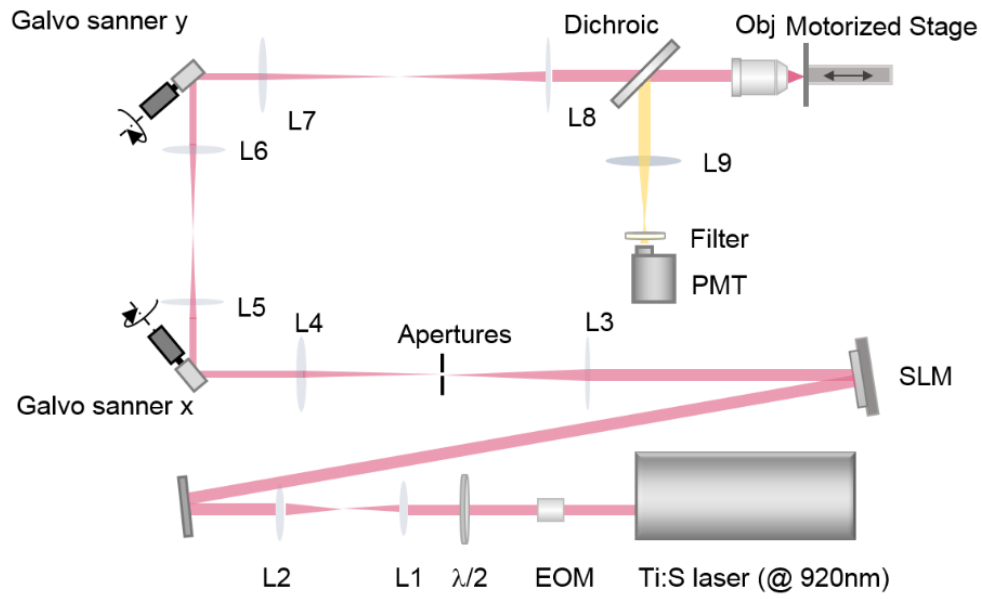


**Fig. S6** Gradient two-photon excitation microscope setup. EOM, electro-optical modulator;  $\lambda/2$ ,  $1/2 \lambda$  wave plate; L, lens; SLM, spatial light modulator; Obj, objective lens; PMT, photomultiplier.



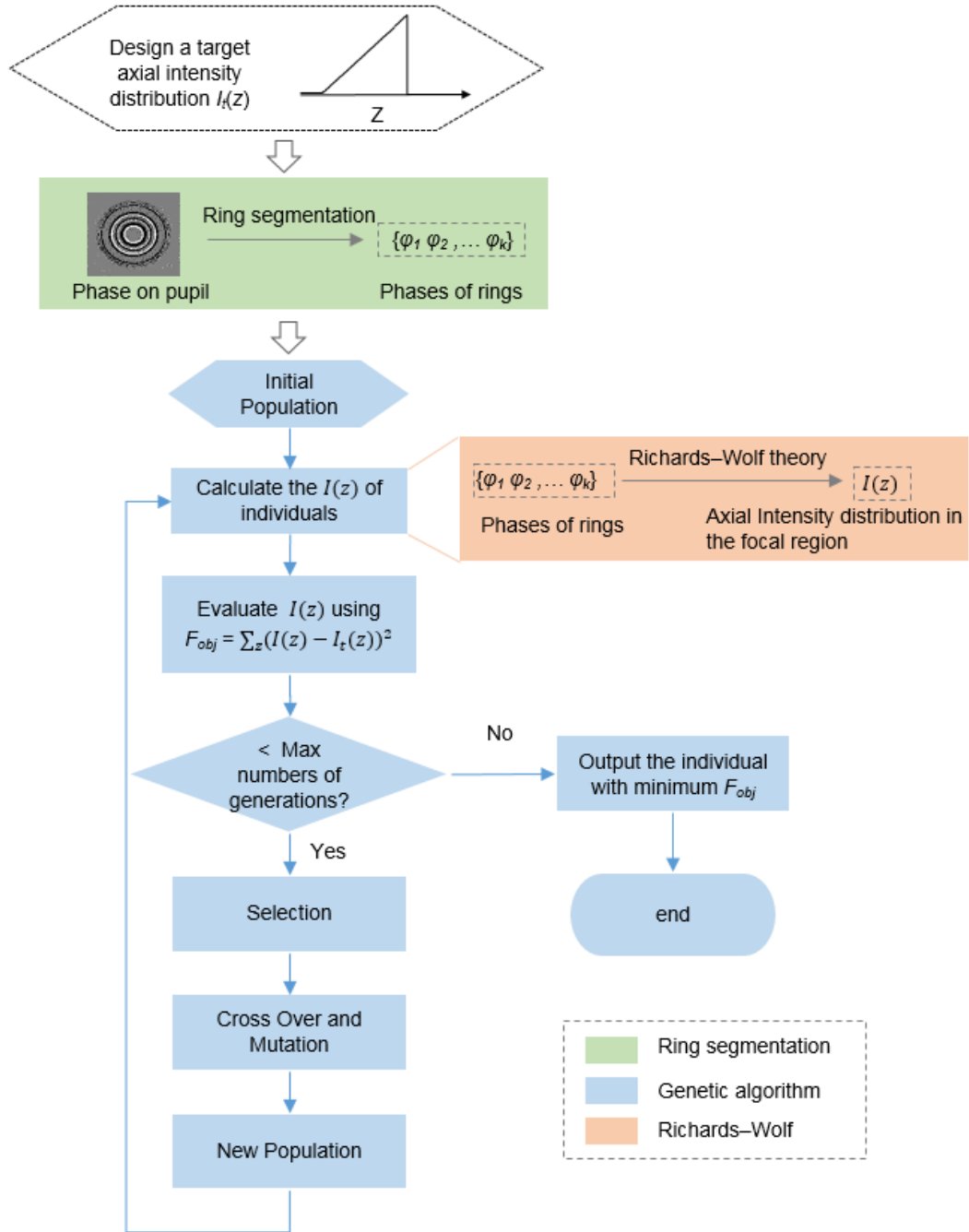


**Fig. S7** Gradient focus generation flowchart.

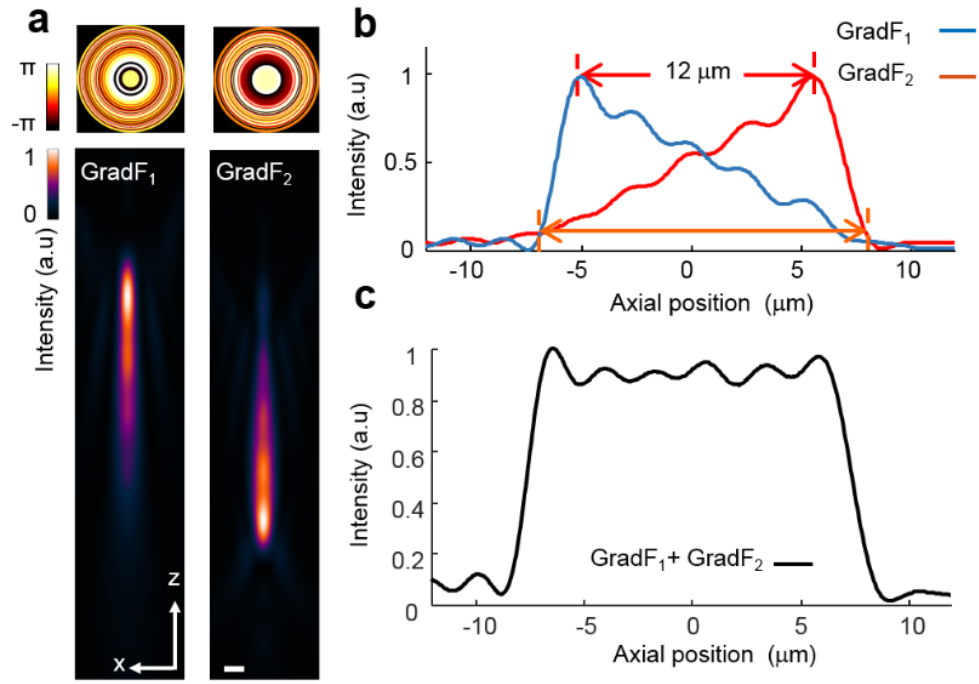


**Fig. S8** Simulated gradient focus pair. **(a)** Axial views of PSFs of pair of gradient foci (GradF<sub>1</sub> and GradF<sub>2</sub>) and corresponding phase patterns that generate PSFs. Scale bar, 1  $\mu\text{m}$ . **(b)** Intensity profiles of two gradient foci along optical axis. **(c)** Sum of axial intensity profiles of gradient focus pair.

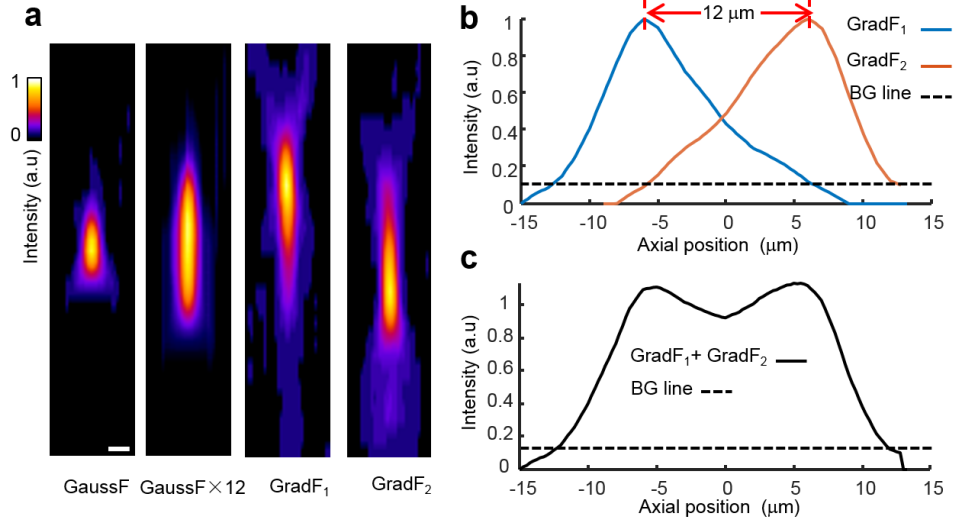


**Fig. S9** Experimental gradient focus pair measured using 1-μm-diameter fluorescent beads. **(a)** Axial-view images of 1 μm fluorescent bead indicating PSF of Gaussian focus (GaussF), axially cascaded Gaussian foci (GaussF × 12), gradient foci 1 and 2 (GradF<sub>1</sub> and GradF<sub>2</sub>, respectively) from left to right. Scale bar, 1 μm. **(b)** Measured intensity profiles of GradF<sub>1</sub> and GradF<sub>2</sub> along optical axis. **(c)** Measured axial intensity profile of sum of GradF<sub>1</sub> and GradF<sub>2</sub>.

We measured the PSF of the gradient focus by performing a 3D scanning of a 1-μm-diameter bead within a voxel size of  $0.25 \mu\text{m} \times 0.25 \mu\text{m} \times 1 \mu\text{m}$ . Because the PSF was undersampled in the axial direction, the resulting PSF was interpolated linearly along the optical axis by a factor of four and then filtered by a 3D Gaussian blur with a radius of one voxel. The square root of the obtained images was used to determine the actual distribution of the excitation light around the focus because the intensity of two-photon excitation fluorescence is proportional to the square of the excitation intensity.

As shown in **b**, the gradient focus exhibits an intensity tail (at the maximum-intensity end) outside the designed axial range. Although we attempted to create an extremely steep tail, some outside fluorophores may still be excited, and their axial locations will be incorrectly estimated. To alleviate this effect, we first adjusted the axial displacement between the pair of foci such that the excitation intensity of one focus is sufficiently small outside the designed axial range. Subsequently, a threshold (BG line in **b**) was empirically selected to exclude the outside fluorophores. Hence, the outside fluorophores excited by the tail at the maximum-intensity end of a focus were located outside of the minimum-intensity end of another focus (under the BG line). These fluorophores will yield an outlier intensity ratio when one of the pairs of intensities becomes negligible. Finally, we carefully determined the intensity ratio range corresponding to the designed axial range and ascribed the fluorophore with an outlier intensity ratio to the nearest available position (top or bottom).

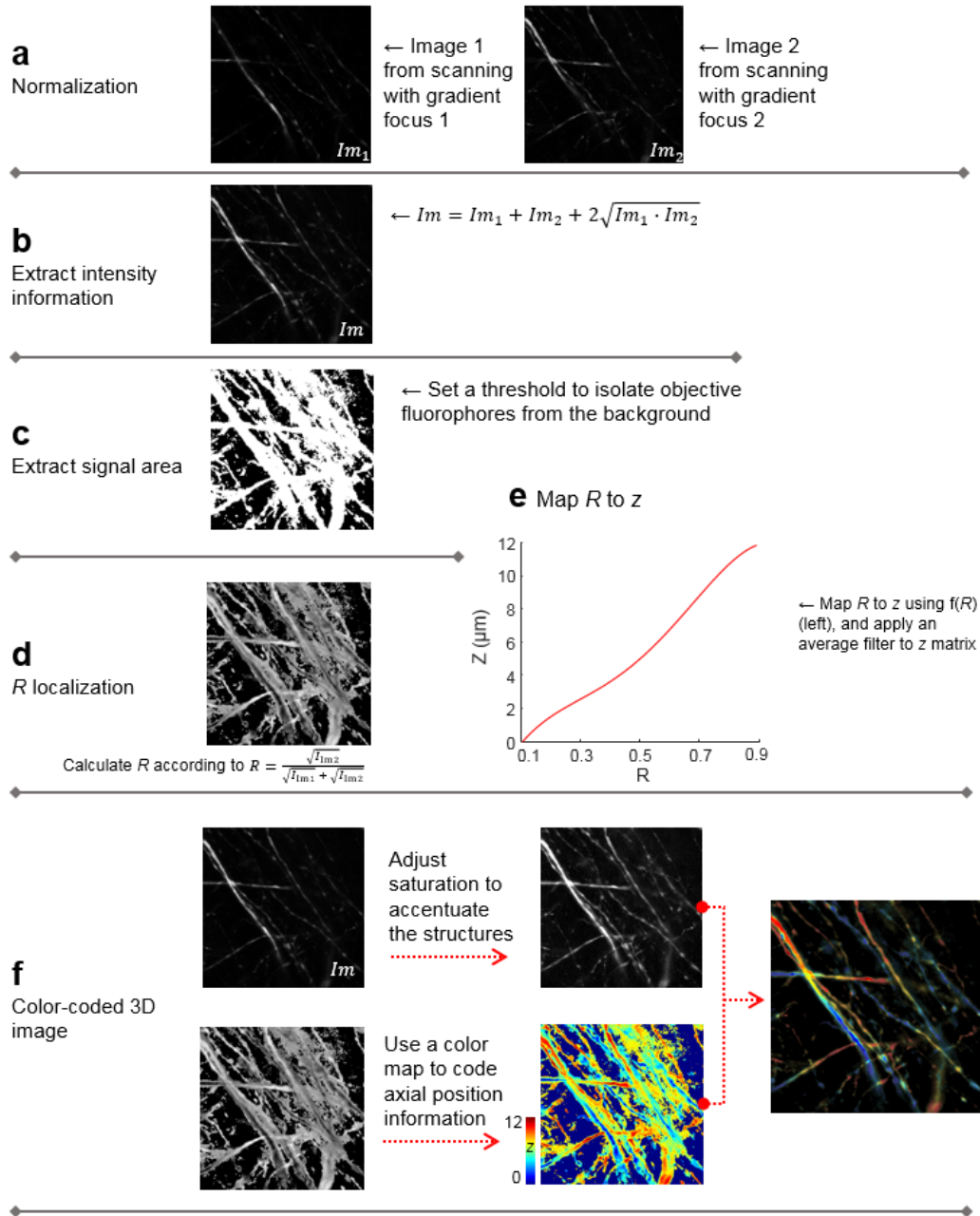


**Fig. S10** Flowchart for axial location information extraction. Unit of  $z$ :  $\mu m$ .

**Table S1.** Data acquisition parameters.

Sample	Figures and Movies	Imaging mode	Volume acquisition speed (s/volume)	Interval time (s)	Volume size ( $\mu\text{m}^3$ )	Excitation power (mW)
Bead	Fig. 1c-f	Gauss-TPM	24	0	50×50×12	2
		Grad-TPM	4	0	50×50×12	6
Brain slice of CX <sub>3</sub> CR1-GFP mouse	Fig. 2	Gauss-TPM	220	0	200×200×22	12
		Grad-TPM	~37	0	200×200×22	~30
HEK293 cell	Fig. 3a and Visualization 1	Gauss-TPM	13	2	100×100×13	~20
		Grad-TPM	2	13	100×100×12	45
RAW264 cell (macrophage)	Fig. 3b and Visualization 3	Grad-TPM	8	2	200×200×12	6
HepG2 cell	Fig. S3 and Visualization 2	Gauss-TPM	52	8	62.5×62.5×13	~20
		Grad-TPM	8	52	62.5×62.5×12	45